Field Gradient Focusing: A Novel Method for Protein Separation

Wendy S. Koegler and Cornelius F. Ivory*

Department of Chemical Engineering, Washington State University, Pullman, Washington 99164-2710

Equilibrium gradient techniques constitute a class of separation methods that combine the steps of separation and concentration by using a gradient in one or more counteracting forces to create a stable equilibrium point at which a protein can focus. Different proteins focus at different equilibrium points, creating a steady-state distribution of isolated proteins. Equilibrium gradient techniques can be adapted to a specific separation by choosing appropriate counteracting forces based on differences in the physical properties of the proteins involved. Zone electric field gradient focusing (FGF) is a new addition to this class of separation techniques with the unique property of using a gradient in the electric field to establish an equilibrium point instead of using a gradient in the velocity or pH. This paper presents two mathematical models which can be used to predict the steady-state concentration profiles obtained by zone electric field gradient focusing. The first model applies only at very low protein concentrations where nonlinear effects can be ignored, e.g., less than 1 mg/mL, but it can be solved analytically and is useful in understanding the basic principles engendered in the method. The second model applies at all concentrations and allows for variations in the electric field strength where the protein focuses, but requires numerical solution. The design of an experimental device is also reported, as well as the results of two experiments: (1) the focusing of the protein hemoglobin from a dilute solution and (2) the separation of different oxidation states of the protein myoglobin.

Introduction

Advances in genetic engineering and cell culture have greatly increased the variety of proteins potentially available for use as pharmaceuticals and diagnostic agents (Jorgenson and Phillips, 1987; Scragg, 1988). This has challenged the bioprocessing industry to find separation techniques that can achieve the requisite high purities and yet be gentle enough to retain the proteins' biological activities. While much work has been done to adapt conventional purification technology to biological product recovery and to scale-up existing laboratory bioseparations, the unique properties of biological products suggest a need for the investigation of novel techniques (Sikdar et al., 1990).

O'Farrell (1985) brought renewed interest to electrochromatography as a preparative-scale method with his paper on counteracting chromatographic electrophoresis (CACE). Perhaps more importantly, he identified CACE as a specific example of a class of methods that work by creating a stable equilibrium point where a solute will "focus" and which could therefore be used to simultaneously isolate and concentrate proteins. Such techniques have been classified as equilibrium gradient methods (Giddings and Dahlgren, 1971) and are generally[1] realized by applying to a solute a set of two (or more) counteracting forces whose net sum changes direction at a unique point in a column. At least one of these must vary gradually so that the net force on the solute acts everywhere in the column to push the solute toward an equilibrium or focal point (see Figure 1). Various approaches have been suggested for producing equilibrium gradient methods, and examples (McCoy, 1986) include using combinations of gravitational, magnetic, and electric fields to generate the opposable forces. A more extensive list of applicable fields is given in Giddings' paper (Giddings, 1984) on two-dimensional separations although this matrix was originally intended for orthogonal rather than opposed fields.

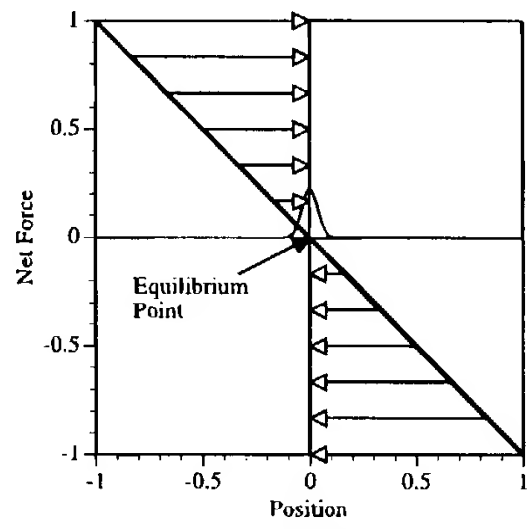

Figure 1. Generic equilibrium gradient focusing example. Solute focuses at the equilibrium point, in this case 0, where the net force acting on it is zero. Upstream (left) of this point, the net force is positive and pushes the solute toward the equilibrium point. Solute located downstream (right) is pushed in the negative direction, again toward the equilibrium point.

Other extant equilibrium gradient techniques include density gradient sedimentation (van Holde, 1971) and isoelectric focusing (IEF; Righetti, 1983). Recent reviews in the electrophoresis literature describe advances made in the application of IEF at analytical (Kuhr and Monnig, 1992), preparative (Righetti et al., 1991; Roman and Brown, 1994), and larger scales (Ivory, 1988; Nath et al., 1993) as well as current research in chromatofocusing (Jungbauer et al., 1990; Sluyterman and Kooistra, 1990; Hjertén et al., 1992), which is closely related to IEF but which, like other forms of gradient elution chromatography, does not require an electrical current. Isota-

[1] Isoelectric focusing is an exception in that it requires only a single, varying force field.

S8756-7938(96)00062-8 CCC: $12.00

chophoresis (ITP; Everaerts et al., 1976; Everaerts and Verheggen, 1987) is a related technique which requires passage of an electric current and which does concentrate and separate solutes. However, because of the special boundary conditions manifested in the use of leading and terminating electrolytes, it cannot be considered an equilibrium gradient technique. ITP's relation to IEF is quite similar to the relationship between displacement chromatography and gradient elution chromatography, both in their physicochemistry and in the mathematics used to describe them.

The following paper examines a new equilibrium gradient method where the variation in the net force is created by establishing a gradient in the electric field. The net force in this technique, named field gradient focusing (FGF), is generated when a gradient in the electrophoretic force is opposed by a constant convective force. FGF is a new addition to the class of equilibrium gradient methods which includes IEF and CACE, and its discovery suggests that other, previously unknown members of this family may exist.

In the following section of this paper, a linear mathematical model of FGF will be presented to outline the basic principles of this technique. This is then followed by a more rigorous model that includes nonlinear effects due to coupling via the electric field. The experimental section of this paper describes an apparatus designed to generate a linear electric field gradient and presents the results of two experiments performed to illustrate how FGF works. The first experiment is the focusing of hemoglobin from a dilute solution to a concentrated band, and the second is the separation of myoglobins with heme irons in different oxidation states.

Theory

A particle in solution will migrate in an electric field with a velocity, v_i, proportional to the charge on that particle, z_i, and the electric field strength, E, such that

$$v_i = z_i \omega_i E \tag{1}$$

where ω_i, is the absolute mobility of the particle. At conditions approaching infinite dilution, the one-dimensional motion of a charged particle can be described by the flux equation

$$J_i(x) = -D_i \frac{\mathrm{d}}{\mathrm{d}x} c_i + (u + z_i \omega_i E(x)) c_i \tag{2}$$

where u is the convective velocity, c_i is the concentration of the ion, and D_i is the dispersion coefficient. Note that u and v_i must have opposite signs if they are to be counteracting as required for focusing. Since we will assume that our x axis is aligned with the flow, this requirement is met if z_i is negative for a positive electric field or if the polarity of the field is reversed. A linear electric field gradient can be described as

$$E(x) = E_1 x + E_0 \tag{3}$$

where E_0 is the average field in the chamber and E_1 is the increase in field strength per unit length.

In the linear model, interactions between the electric field and buffer ion concentrations are assumed to be negligible. At steady-state, the net flux is zero and eqs 2 and 3 can be integrated to obtain the following concentration distribution:

$$c_i(x) = k \exp\left[\frac{1}{D_i}\left((u + z_i \omega_i E_0)x + \frac{1}{2} z_i \omega_i E_1 x^2\right)\right] \tag{4}$$

The constant of integration, k, is found by placing an integral constraint on the total amount of protein present in the column. If A is the cross-sectional area of the chamber, then the total moles of the ith protein, M_i, can be found by integrating its concentration over the length of the column. Assuming that the concentration approaches zero at the boundaries, the limits on the integration can be replaced by plus or minus infinity to simplify the integration, or

$$M_i = A\int_{-L}^{L} c_i(x)\,\mathrm{d}x \approx A\int_{-\infty}^{\infty} c_i(x)\,\mathrm{d}x \tag{5}$$

Using eq 5 to solve for k, the concentration profile for species i is now given by

$$c_i(x) = \frac{M_i}{A}\sqrt{-\frac{z_i \omega_i E_1}{2\pi D_i}} \exp\left[\frac{z_i \omega_i E_1}{2D_i}\left(x + \frac{u + z_i \omega_i E_0}{z_i \omega_i E_1}\right)^2\right] = \frac{1}{\sqrt{2\pi}} \frac{M_i}{\sigma_i A} \exp\left[-\frac{(x - \chi_{f,i})^2}{2\sigma_i^2}\right] \tag{6}$$

which is a Gaussian distribution with focal point χ and variance σ^2 given by

$$\chi_{f,i} = -\frac{u + z_i \omega_i E_0}{z_i \omega_i E_1} \tag{7}$$

$$\sigma_i^2 = -\frac{D_i}{z_i \omega_i E_1} \tag{8}$$

This model, although simple, yields some very important information. First, the negative sign in the square-root indicates that, in order to achieve stable equilibrium, z_i and E_1 must be of opposite sign. The variance, which is a measure of the width of the focused protein peak, suggests that the focused protein band will be tighter and more concentrated if the dispersion coefficient is decreased or if the electric field gradient is increased. Equation 7 indicates that the flow rate and the average electric field are the main factors in determining the location of the protein peak. However, since the slope of the electric field appears in the denominator of χ, increasing the electric field gradient will have the effect of moving the focused bands closer together. As one might expect, there is a trade-off between increasing concentration and resolution.

The model derived above applies only at low protein concentrations when the buffer ion concentrations and the electric field gradient are unaffected by the presence of focused protein. It is well-known that the local conductivity changes as protein concentration increases and this will alter the local electric field and change the shape and location of the protein peak. Having illustrated the theoretical basis for FGF, a practical means for generating an electric field gradient is now described. This will be followed by the development of a more rigorous model which takes into account coupling of the transport equations by the electric field.

Electric Field "Shaping". The idea of using nonuniform electric fields to enhance electrophoresis is not original to this paper. It is generally accepted that, in a homogeneous, isothermal conducting medium, the current streamlines (equivalent to flow streamlines in an inviscid liquid) will conform to the shape of the vessel through which they pass. This concept has been used by a number of researchers in media which include wedge-shaped gels (Boncinelli et al., 1983) in which the gel thickness is varied, pie-shaped gels (Rolchigo and

Graves, 1988) in which the breadth of the gel is varied, and annular chambers with radially varying fields (Southern, 1979; Mattock et al., 1980).

Pohl (1978) used shaped electrodes to generate the spatial field gradients needed for his work in dielectrophoresis. Cantor and Schwartz (Schwartz and Cantor, 1984) used an array of electrodes with temporal cycling of the voltages to separate large DNA fragments. As a final example, Pawliszyn (Pawliszyn and Wu, 1993) used Joule heating in a cone-shaped capillary to generate temperature gradients which then induced pH gradients in a 50 mM Tris buffer. It is only in this last case that a shaped electric field is used, indirectly, to focus solutes. In this case, the electric field gradient is not an essential part of the method since the thermal gradient could have been generated by other means (Lochmüller and Ronsick, 1991).

In the version of FGF described here, the field gradient is created by varying the area through which the electric current flows. At constant buffer concentrations, the local electric field is roughly related to the total current, I, passing through a chamber by

$$E(x) = \frac{I}{\sigma A(x)} \tag{9}$$

where σ is the conductivity of the buffer and $A(x)$ is the cross-sectional area of the chamber. Simply varying the cross-sectional area of the column to generate the electric field gradient would alter the fluid flow rate in a way that would effectively compensate the focusing effect due to electric field shaping. This problem is solved by dividing the chamber into two regions separated by a membrane which is permeable to the current but not to bulk fluid flow (see Figure 2). The cross-sectional area on the protein side of the membrane is fixed so that the flow rate in this region is constant. Current can cross the membrane (via the buffer ions), and so the current density is shaped by the total cross-sectional area of the chamber.

An expression for the variation in area needed to create a linear electric field can be found by substituting eq 3 into eq 9 and solving for $A(x)$. Once the equipment is built, however, the area is independent of experimental conditions and it is more useful to describe the area with the following equation:

$$A(x) = \frac{2A_T A_B}{\frac{x}{L}(A_T - A_B) + (A_T + A_B)} \tag{10}$$

where A_T and A_B are the total areas at the top and bottom of the chamber.

The experimental apparatus consists of a shaped Plexiglas outer shell and an inner cylinder of dialysis membrane tubing. Focusing of proteins occurs in a packed bed inside the dialysis tubing, and the buffer circulating through the annular space serves double duty as a coolant (Figure 7).

Nonlinear Model Derivation. A minimal nonlinear model consists of three regions, each with three components and a variable electric field. The three components are the protein, the buffer cation, and the buffer anion, denoted by the subscripts p, $+$, and $-$, respectively. Region 1 is the volume inside the dialysis membrane where a protein will be focused and is of constant cross-sectional area, A_1. Region 2 is the annular space between the shaped Plexiglas shell and the dialysis membrane and has variable area, $A_2(x)$, equal to the total area described in eq 10 minus A_1. The third region is the

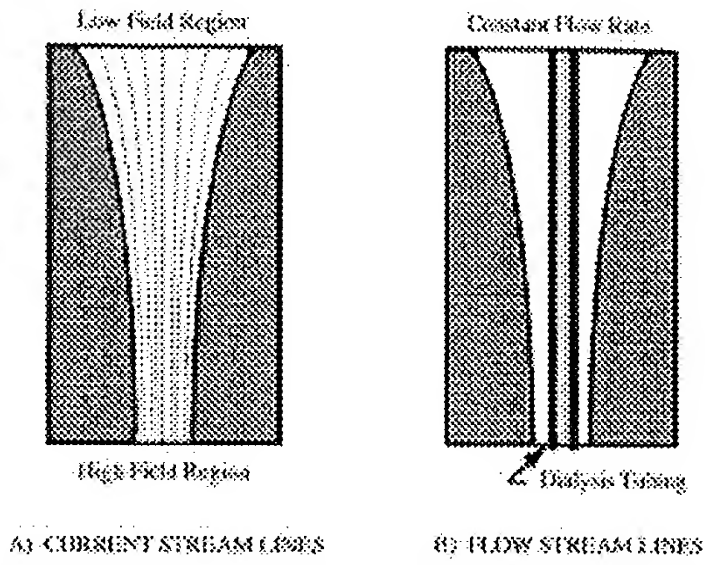

Figure 2. Current and flow stream lines. The electric field is shaped by varying the area through which the current flows. (A) As the area decreases, the current density increases, as does the electric field strength. Small ions will carry the current across the membrane so that the total area shapes the field. (B) The flow rate inside the dialysis tubing remains constant because there is no bulk fluid flow of buffer across the membrane.

membrane, of thickness δ, between regions 1 and 2 and will be denoted by a subscript m. Buffer ions are free to cross the membrane and can be found in all three regions. The protein cannot enter the membrane, which has a molecular weight cutoff below 12 kD, and so will only be found in region 1.

The chamber has length $2L$ with position along the axis denoted by x and with the origin located at the center. (The chamber is actually oriented vertically with the top located at $-L$). It is assumed that radial concentration gradients in region 1 can be ignored and plug flow is assumed since region 1 will be packed. Externally cooled buffer is assumed to flow through region 2 fast enough that the buffer concentrations there are essentially constant. The concentration of buffer ions in the membrane will depend on both x and r. The membrane is assumed to be thin enough that it can be analyzed in Cartesian coordinates, and y will denote the radial location in the membrane. The electric field is assumed to be constant across the radial axis in all regions at any point x. Finally, it is assumed that the concentrations of hydronium and hydroxyl ions are negligible compared with the buffer ions and that the ionized portion of the buffer can be treated as a strong, binary electrolyte, i.e., no local shift in the buffer pH is allowed.

The basic equations needed for this derivation include the molar flux, written now as the flux of a the ith component in the kth region, or

$$\vec{J}_{ik} = -D_i \nabla c_{ik} + (\vec{u}_k + \mu_i \vec{E}) c_{ik} \tag{11}$$

where the ionic mobility, μ_i, is equal to $z_i \omega_i$. The current density for the kth region is

$$\vec{i}_k = F \sum_{i=1}^{N_k} z_i \vec{J}_{ik} \tag{12}$$

where N_k is the number of components in the kth region. The current density is related to the total current by

$$\vec{I}_T = \sum_{k=1}^{K} A_k \vec{i}_k \tag{13}$$

where K is the total number of regions and A_k is the area

of the *k*th region. The condition of electroneutrality must hold locally for each region, so

$$\sum_{i=1}^{N_k} z_i c_{ik} = 0 \tag{14}$$

These equations will be used to model the steady-state behavior of each component and the electric field following the assumptions described above. However, because the components of each region are coupled by electroneutrality, eq 14, one component can be substituted out of the system of equations in each region. In this derivation, the anion is eliminated.

The expressions for the cation and protein concentrations are derived from a general differential mole balance on region 1 where $J_{i1}(x)$ is the flux of component i in the axial direction and $J_{im}(x)$ is the flux of i across the membrane at point x

$$-\frac{d}{dx}J_{i1}(x) - \frac{W}{A_1}J_{im}(x) = 0 \tag{15}$$

and W is the width of the interfacial area, in this case the circumference of the dialysis tube. Note that, because radial concentration gradients in region 1 have been assumed to be negligible, the ion flux across the membrane shows up in eq 15 as a homogeneous source/sink.

For a protein which cannot enter the membrane, $J_{pm}(x) = 0$, and eq 15 simplifies to

$$0 = \frac{d}{dx}J_{p1}(x) = \frac{d}{dx}\left(-D_p\frac{d}{dx}c_{p1}(x) + (u_1 + \mu_p E(x))\, c_{p1}(x)\right) \tag{16}$$

Two boundary conditions are needed to solve this second-order differential equation. The first is that the flux of protein into the column is zero,

$$J_{p1}(-L) = -D_p\frac{d}{dx}c_{p1}(x) + (u_1 + \mu_p E(x))\, c_{p1}(x) = 0 \tag{17}$$

and the second boundary condition is supplied in the form of a constraint on the total amount of protein loaded into region 1:

$$M_{p1} = \int_{-L}^{L} A_1\, c_{p1}(x) \tag{18}$$

where M_{pT} is the total moles of protein in region 1 of the chamber. This integral equation can be converted to a differential equation

$$\frac{d}{dx}M_p(x) = A_1\, c_{p1}(x) \tag{19}$$

with boundary conditions

$$M_p(-L) = 0 \tag{20}$$

$$M_p(L) = M_{p1} \tag{21}$$

Equation 19 is a first-order equation and needs only one of these conditions. The last condition is used as an additional boundary condition for the protein mole balance, eq 16. The mole balance on the protein now consists of two coupled differential equations and three boundary conditions. The reason for converting the integral constraint to a differential equation is to simplify the implementation of a differential equation solver.

To complete the general mass balance for the cation in region 1 (eq 15), an expression for the flux across the membrane is needed. To avoid the need to solve partial differential equations, the axial flux in the membrane is assumed to be negligible in comparison to the radial flux across the membrane. This is a good approximation if the membrane is very thin or if the axial concentration gradients in the membrane are negligible compared with the concentration difference across the membrane. A steady-state mole balance across the membrane yields

$$\frac{\partial}{\partial y}J_{im} = 0 \tag{22}$$

Given these assumptions, the flux across the membrane is a function of x only and is given by

$$J_{im} = f_{i1}(x) = -D_{im}\frac{\partial}{\partial y}c_{im}(x,y) + \mu_{im}\, E_m(x)\, c_{im}(x,y) \tag{23}$$

There is no bulk flow across the membrane so the convective term has been dropped from the flux expression. Furthermore, D_{im} is not a dispersion coefficient, since there is no convective flow in the membrane, but is instead a molecular diffusion coefficient. E_m is the component of the electric field in the radial direction and is assumed to be independent of y. The current density flowing through the membrane at x can be found by summing the fluxes of ions across the membrane

$$i_m(x) = F\sum_{i}^{N_m} z_i J_{im} = F\left(-\sum_{i}^{N_m} z_i D_{im}\frac{\partial}{\partial y}c_{im}(x,y) + E_m(x)\sum_{i}^{N_m} z_i\mu_{im}\, c_{im}(x,y)\right) \tag{24}$$

where N_m is the number of components in the membrane, e.g., two for a binary electrolyte. Solving for the electric field in the membrane and substituting out the anion concentration using electroneutrality yields the expression

$$E_m(x) = \frac{i_m(x) + Fz_{+m}(D_{+m} - D_{-m})\frac{\partial}{\partial y}c_{+m}(x,y)}{Fz_{+m}(\mu_{+m} - \mu_{-m})\, c_{+m}(x,y)} \tag{25}$$

The cation flux across the membrane can now be written

$$J_{+m}(x) = f_{+1}(x) = \frac{\mu_{-m}D_{+m} - \mu_{+m}D_{-m}}{\mu_{+m} - \mu_{-m}}\frac{\partial}{\partial y}c_{+m}(x,y) + \frac{\mu_{+m}\, i_m(x)}{Fz_{+m}(\mu_{+m} - \mu_{-m})} \tag{26}$$

and the concentrations at the membrane boundaries must be continuous, so the boundary conditions on the membrane are

$$c_{+m}(x,0) = c_{+1}(x) \tag{27}$$

$$c_{+m}(x,\delta) = c_{+2} \tag{28}$$

Integrating and applying the boundary conditions re-

duces the concentration profile to a linear gradient through the membrane

$$c_{+m}(x,y) = [c_{+2} - c_{+1}(x)]\frac{y}{\delta} + c_{+1}(x) \tag{29}$$

and the cation mole flux through the membrane becomes

$$J_{+m}(x) = \left(\frac{\mu_{-m}D_{+m} - \mu_{+m}D_{-m}}{\mu_{+m} - \mu_{-m}}\right)\left(\frac{c_{+2} - c_{+1}(x)}{\delta}\right) + \frac{\mu_{+m}\, i_m(x)}{Fz_{+m}(\mu_{+m} - \mu_{-m})} \tag{30}$$

To find i_m, a current balance must be performed. A differential current balance in region 2 yields

$$-\frac{d}{dx}(A_2(x)\, i_2(x)) + W\, i_m(x) = 0 \tag{31}$$

Rearranging and using eq 12 for the current density in region 2, the charge flux across the membrane becomes

$$i_m(x) = \frac{F}{W}\frac{d}{dx}(A_2(x)(\sum_{i=1}^{N_2} z_{i2}\, u_2(x)\, c_{i2} + \sum_{i=1}^{N_2} z_{i2}\mu_i\, E(x)\, c_{i2})) \tag{32}$$

where N_2 is the number of components in region 2. The dispersion term is left out of the flux equation for region 2 because there are no concentration gradients. Also, the velocity in region 2 is a function of x due to the changing area. If the parameters independent of i are factored out of the summations, it can be seen that the first summation becomes zero due to electroneutrality and that the second summation is the conductivity times the electric field. Substituting out the anion using the electroneutrality relation for region 2 gives the current density in the membrane at point x as

$$i_m(x) = \frac{Fz_+(\mu_+ - \mu_-)}{W}c_{+2}\frac{d}{dx}(A_2(x)\, E(x)) \tag{33}$$

A mole balance on the cation in region 1 can now be assembled to give

$$A_1\frac{d}{dx}\left(-D_+\frac{d}{dx}c_{+1}(x) + (u_1 + \mu_+ E(x))\, c_{+1}(x)\right) + \frac{W(\mu_{-m}D_{+m} - \mu_{+m}D_{-m})}{\delta(\mu_{+m} - \mu_{-m})}(c_{+2} - c_{+1}(x)) + \frac{c_{+2}\mu_{+m}(\mu_+ - \mu_-)}{\mu_{+m} - \mu_{-m}}\frac{d}{dx}(E(x)\, A_2(x)) = 0 \tag{34}$$

where the first term describes the movement of cations in region 1, the second term describes the movements of ions across the membrane due to diffusion, and the third term describes the cations carried across the membrane by the current. The two boundary conditions needed for this second-order differential equation are supplied by specifying that the concentrations at the inlet and outlet to the chamber are the same as those in the recirculating buffer, i.e.

$$c_{+1}(-L) = c_{+1}(L) = c_{+2} \tag{35}$$

The last step in this derivation is to find an expression for the electric field. This procedure is similar to that followed in finding E_m for the cation flux across the membrane. The total current is related to the total charge flux by

$$I_T = A_1 i_1 + A_2(x) i_2 = A_1 F\sum_{i=1}^{N_1} z_i J_{i1} + A_2(x)\, F\sum_{i=1}^{N_2} z_i J_{i2} \tag{36}$$

where N_k is the number of components in region k. The second summation reduces to the electric field times the conductivity in region 2, as seen in the derivation of i_m. Substituting for the flux in region 1 and solving for the electric field, the equation becomes

$$E(x) = \frac{I_T + A_1 F\sum_{i=1}^{N_1} z_i D_i \frac{d}{dx}c_{i1}(x)}{A_1 F\sum_{i=1}^{N_1} z_i\mu_i\, c_{i1}(x) + A_2(x)\, F\sum_{i=1}^{N_2} z_i\mu_i c_{i2}} \tag{37}$$

The velocity terms disappear because of electroneutrality, and the anion can be substituted out using electroneutrality for region 1, which includes the protein, to yield

$$c_{-1}(x) = -\frac{z_+}{z_-}c_{+1}(x) - \frac{z_p}{z_-}c_{p1}(x) \tag{38}$$

The electric field equation is now given by

$$E(x) = \frac{\frac{I_T}{F} + A_1\left(z_+(D_+ - D_-)\frac{d}{dx}c_{+1}(x) + z_p(D_p - D_-)\frac{d}{dx}c_{p1}(x)\right)}{A_1(z_+(\mu_+ - \mu_-)\, c_{+1}(x) + z_p(\mu_p - \mu_-)\, c_{p1}(x)) + A_2(x)\, z_+(\mu_+ - \mu_-)c_{i2}} \tag{39}$$

At this point the nonlinear model consists of a system of four simultaneous differential equations which must be solved for the variables $c_{p1}(x)$, $M_p(x)$, $c_{+1}(x)$, and $E(x)$. After these equations are solved, $c_{-1}(x)$ can be found from the electroneutrality relation, eq 38.

Extension to Multiple Proteins. The mole balance on a second protein, q, has the same form as the mole balance on p

$$\frac{d}{dx}J_{q1}(x) = \frac{d}{dx}\left(-D_q\frac{d}{dx}c_{q1}(x) + (u_1 + \mu_q E(x))\, c_{q1}(x)\right) = 0 \tag{40}$$

and a similar total mole constraint

$$\frac{d}{dx}M_q(x) = A_1\, c_{q1}(x) \tag{41}$$

along with the boundary conditions

$$J_{q1}(-L) = -D_q\frac{d}{dx}c_{q1}(x)|_{x=-L} + [u_1 + \mu_q E(-L)]\, c_{q1}(-L) = 0 \tag{42}$$

$$M_q(-L) = 0 \tag{43}$$

$$M_q(L) = M_{qT} \tag{44}$$

The only other quantities affected are the summations over region 1 in the electric field, eq 37, and the charge balance, eq 38.

Nondimensional Analysis. The system of equations can be put in dimensionless form by defining the following variables:

$$\zeta = \frac{x}{L} \tag{45}$$

$$p(\zeta) = \frac{c_{p1}(x)}{c_{p,\mathrm{av}}} \tag{46}$$

$$M(\zeta) = \frac{M_p(x)}{M_{p\mathrm{T}}} \tag{47}$$

$$c(\zeta) = \frac{c_{+1}(x)}{c_{+2}} \tag{48}$$

$$E(\zeta) = \frac{E(x)}{E_0} \tag{49}$$

$$a(\zeta) = \frac{c_{-1}(x)}{c_{-2}} \tag{50}$$

where

$$c_{p,\mathrm{av}} = \frac{M_{p\mathrm{T}}}{2A_1 L} \tag{51}$$

and

$$E_0 = \frac{I_\mathrm{T}}{F c_{+2} z_+ (\mu_+ - \mu_-)\, A(0)} \tag{52}$$

The equation for the characteristic electric field foreshadows the trend for the dimensionless numbers to be ratios of parameters based on (1) the buffer conductivity and (2) the average of the total area of the chamber, as given by eq 10, evaluated at zero. Nondimensionalizing the protein mole balance yields

$$\frac{\mathrm{d}}{\mathrm{d}\zeta}\left(-\frac{1}{N_{\mathrm{Pe},p}}\frac{\mathrm{d}}{\mathrm{d}\zeta}p(\zeta) + \left(1 - \frac{1}{\gamma_p}E(\zeta)\right)p(\zeta)\right) = 0 \tag{53}$$

where

$$N_{\mathrm{Pe},p} = \frac{Lu_1}{D_p} \tag{54}$$

$$\gamma_p = -\frac{u_1}{\mu_p E_0} \tag{55}$$

The Peclet number, $N_{\mathrm{Pe},p}$, is a ratio of the convective flow to dispersion in the column. The second dimensionless number, γ, is the ratio of the convective velocity to the average electrophoretic velocity in the column and indicates the location of a peak in the chamber (where the two forces balance). Because the ionic mobility and the electric field have opposite signs, γ_p, will be a positive number.

Nondimensionalizing the mole constraint, eq 19, yields

$$\frac{\mathrm{d}}{\mathrm{d}\zeta}M(\zeta) = \frac{1}{2}p(\zeta) \tag{56}$$

In the cation mole balance and the electric field equation, the relative mobilities of the ions become important. Dimensionless mobilities are defined as

$$t_+ = \frac{\mu_+}{\mu_+ - \mu_-} \tag{57}$$

$$t_- = -\frac{\mu_-}{\mu_+ - \mu_-} \tag{58}$$

$$t_p = -\frac{\mu_p}{\mu_+ - \mu_-} \tag{59}$$

Note that the mobilities of the anion and the protein are both negative so that, in the above equations, both terms in the denominator are positive and all three of the dimensionless numbers are positive. Equations 56 and 57 resemble the transference numbers of a solution, which represent the fraction of the current being carried by each ion. They sum to 1 and are not independent. The mobility of an ion is related to its molecular diffusion coefficient by the Nernst–Einstein equation

$$D_i = RT\omega_i \tag{60}$$

so that the transference numbers in the membrane can be written

$$t_{+\mathrm{m}} = \frac{\mu_{+\mathrm{m}}}{\mu_{+\mathrm{m}} - \mu_{-\mathrm{m}}} = \frac{D_{+\mathrm{m}}}{D_{+\mathrm{m}} + D_{-\mathrm{m}}} = 1 - t_{-\mathrm{m}} \tag{61}$$

The mole balance on the cation can be nondimensionalized to

$$\frac{\mathrm{d}}{\mathrm{d}\zeta}\left(-\frac{1}{N_{\mathrm{Pe},+}}\frac{\mathrm{d}}{\mathrm{d}\zeta}c(\zeta) + \left(1 + \frac{t_+ E(\zeta)}{\gamma_p t_p}\right)c(\zeta)\right) - \frac{(1 - t_{+\mathrm{m}})D_{\mathrm{R}+}K}{N_{\mathrm{Pe},+}R_1}(1 - c(\zeta)) + \frac{t_{+\mathrm{m}}}{\gamma_p t_p}\frac{\mathrm{d}}{\mathrm{d}\zeta}(E(\zeta)A_\mathrm{R}(\zeta)) = 0 \tag{62}$$

where

$$A_\mathrm{R}(\zeta) = \frac{A_2(\zeta)}{A_1} \tag{63}$$

$$R_1 = \frac{A_1}{A(0)} \tag{64}$$

$$D_{\mathrm{R}+} = \frac{D_{+\mathrm{m}}}{D_+} \tag{65}$$

$$K = \frac{L}{\delta}\frac{2LW}{A(0)} \tag{66}$$

$A_\mathrm{R}(z)$ is the ratio of the cross-sectional area of region 2 to that of region 1. R_1 is a measure of the fraction of the total cross-sectional area occupied by region 1. R_m represents the total change of area in the chamber and, because the area and electric field are related, also represents the ratio of the slope of the electric field to its average value. $D_{\mathrm{R}+}$ is the ratio of diffusion in the membrane to the dispersion in the column. K is the ratio of a dimensionless membrane thickness with the ratio of membrane area to the total area.

Nondimensionalizing the electric field equation gives the equation

$$E(\zeta) = \frac{\frac{1}{R_1} + \gamma_p t_p \left(\left(\frac{1}{N_{Pe,+}} - \frac{1}{N_{Pe,-}} \right) \frac{d}{d\zeta} c(\zeta) - e_R \left(\frac{1}{N_{Pe,p}} - \frac{1}{N_{Pe,-}} \right) \frac{d}{d\zeta} p(\zeta) \right)}{c(\zeta) + e_R (t_p - t_-)\, p(\zeta) + A_R(\zeta)} \tag{67}$$

which yields one last dimensionless parameter

$$e_R = -\frac{Z_p c_{p,av}}{Z_+ c_{+2}} \tag{68}$$

Inspection of the dimensionless electric field equation reveals that as e_R approaches zero, i.e., the amount of protein in the system is very small, all terms containing the protein concentration drop out of the electric field equation so its solution will be the same as for the linear model derived earlier.

The five dimensionless boundary conditions are

$$-\frac{1}{N_{Pe,p}} \frac{d}{d\zeta} p(\zeta)|_{z=-L} + \left(1 - \frac{1}{\gamma_p} E(-L)\right) p(-L) = 0 \tag{69}$$

$$M_p(-L) = 0 \tag{70}$$

$$M_p(L) = 1 \tag{71}$$

$$c(-L) = c(L) = 1 \tag{72}$$

And finally, the steady-state concentration profile for the anion can be calculated as

$$a(\zeta) = c(\zeta) - e_R\, p(\zeta) \tag{73}$$

The equations were solved using a FORTRAN subroutine called ODECOL, which was written by W. A. Gobie and solves boundary-value problems using orthogonal collocation on finite elements. ODECOL is similar in structure and use to COLSYS (Ascher et al., 1981), a well-known collocation program that also solves boundary-value ordinary differential equations.

The effects of the identified dimensionless parameters on the focusing of a single-protein peak were estimated by varying each one separately in comparison to a base model (Koegler, 1994). A few examples are given in Figures 3–6.

Due to the large number of dimensionless parameters in the model, a few assumptions were made to simplify the analysis. Because dispersion in a packed column may be estimated as the product of the solvent velocity times the bed particle diameter, the Peclet numbers for all components were assumed to be the same in a packed column. If the membrane mobilities of the buffer cation and anion differ from their free solution mobilities by the same factor, e.g., the porosity of the membrane, this factor would drop out of a ratio of mobilities so that $t_{+m} = t_+$. K was estimated from the geometry of the apparatus to be about 70 000.

Figure 3 demonstrates how the steady-state concentration and the electric field profiles deviate from the simple, Gaussian distribution predicted by the linear model as the amount of protein in the system, i.e., e_R, is increased. When a negatively charged protein focuses, the buffer anion is excluded from the focused band due to electroneutrality effects and the local conductivity changes. If the protein has a smaller mobility than the anion, as in Figure 3, the local conductivity will decrease and the local field strength will increase. This acts to distort or "hump" the field so that the upstream side of the protein peak experiences a steeper gradient in the electric field and sharpens, while the downstream side experiences a relatively flat field and spreads out or tails. The opposite occurs when the protein is faster than the displaced co-ion.

In Figure 4, the trade-off between high concentration and ease of separation is illustrated. When the electric field gradient is very steep, protein peaks become tighter and, hence, more concentrated. However, they will also be forced closer together resulting in lower resolution. A shallow gradient allows greater resolution, but at lower protein concentrations.

Figure 5 shows that the location of the focused protein band within the chamber can affect the degree of separation. This comes about because the ratio of the forces acting on the protein is not constant throughout the chamber. It should also be noted that peaks of the proteins with smaller mobilities, like protein q, will be more dispersed for similar reasons.

At first, increasing the Peclet number results in behavior predicted by the simple Gaussian distribution. The protein peaks tighten until a Peclet number of about 200 is reached. However, when the Peclet number is increased above 200, the peaks begin to broaden while at the same time sharpening their forward edges. Also, two proteins focusing near each will tend to exclude each other and "stack out" as shown in Figure 6. At this point, the electric field no longer resembles a linear gradient, but is instead more like a step function where the dimensionless field strength at each step is equal to the γ of the protein focused there.

Experimental Results

Equipment. The basis for the design of the FGF chamber is to divide the shaped chamber into two concentric regions separated by a membrane which is permeable to the electrical current but not to bulk fluid flow. The apparatus consisted of 6.4 mm wet diameter dialysis tubing (BioDesign) mounted in the center of a shaped Plexiglas cylinder (see Figure 7). The assembly consisted of four interlocking Plexiglas pieces sealed by O rings. The open ends of the membrane tubing are slipped over the ends of the mounts and held in place by a collars fitted with an O ring.

Two platinum electrodes, one mounted at the bottom of the outer Plexiglas shell and the second attached to the top, were located in the annular space through which the externally cooled electrolyte buffer flowed. The location of electrodes and the directions of flows are also depicted in Figure 7. Buffer was supplied to the bed using a syringe pump, and proteins were loaded via a sample loop located just above the entrance to the bed.

The dialysis tubing was packed with ToyoPearl HW040F size exclusion resin with a nominal particle size of 45 μm and an exclusion limit of 10 000 Da. The bed was slurry-packed using an open 60 mL syringe screwed into the top port of the bed. When the level of the bed reached the fitting port, the syringe was removed and the bed pressurized to about 5 psi. The remaining volume of the bed was packed via the sample loop to maintain the pressure. The Teflon tubing at the entrance to the bed was wide bore (0.03 in. i.d.) so that the packing could flow through. The bed was supported at the bottom by a cotton plug filling the bore of the bottom mount, but the top surface of the bed was free. The working buffer flowed downward to prevent fluidization.

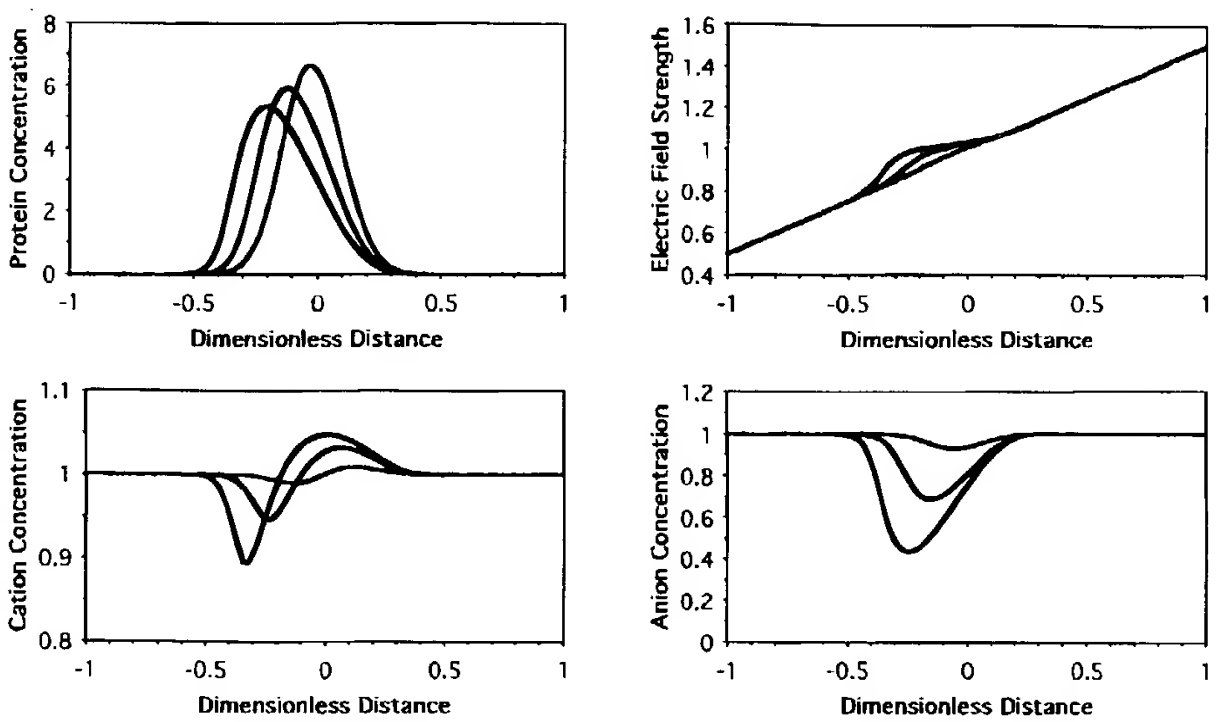

Figure 3. Effect of changing the protein loading for a negatively-charged protein whose electrophoretic mobility is lower than that of the co-ion ($t_p = 0.1$) (e_R is increased from 0.01 to 0.05 and 0.1). As more protein is added to the column, the focused band skews forward, taking on a triangulated shape which is similar to that found with overloaded chromatography peaks. Both anion and cation concentrations are reduced by exclusion effects and the electric field is slightly perturbed in the neighborhood of the focused protein band. In this example, $D_{R+} = 0.1$, $N_{Pe,I} = 150$, $R_I = R_m = t_+ = t_{+m} = 0.5$, and $\gamma_p = 1.0$.

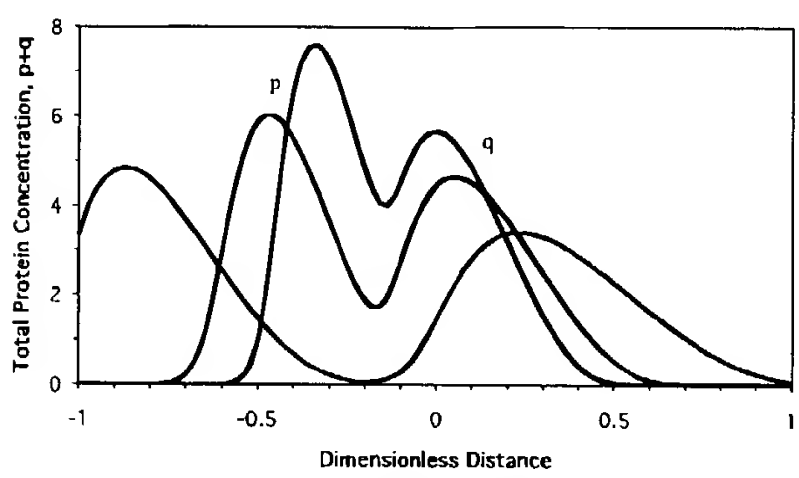

Figure 4. Effect of changing the slope of the electric field on the separation of two proteins with a 30% difference in mobility (increasing R_m from 0.25 to 0.5 and 0.75). Steep electric field gradients produce more concentrated peaks while shallow gradients give better peak resolution. In this example, $t_p = 0.1$, $t_q = 0.07$, $\gamma_p = 0.85$, and $\gamma_q = 1.2$. $D_{R+} = 0.1$, $N_{Pe,I} = 150$, $e_I = 0.1$, and $R_I = t_+ = t_{+m} = 0.5$.

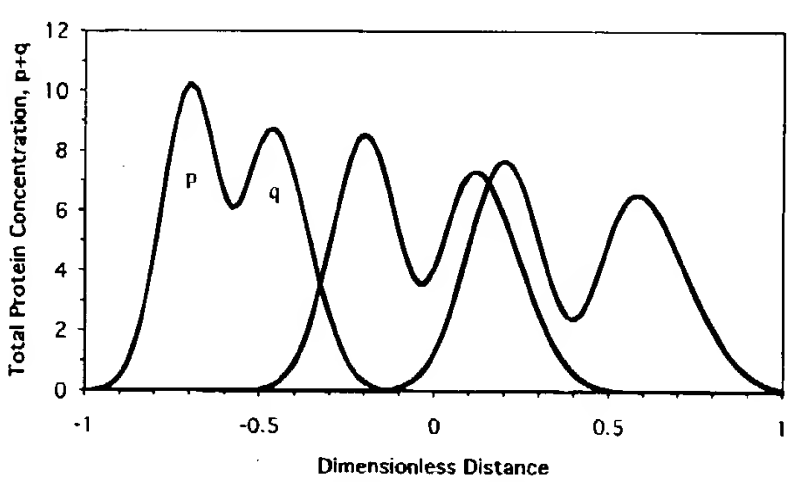

Figure 5. Effect of changing γ_p, the ratio of the convective velocity to the electrophoretic velocity, on the separation of two proteins with a 20% difference in mobility (γ_p from 0.65 to 0.9 and 1.1). As the convective flow increases, the protein peaks are pushed further downstream. The increased dispersion is due to the effect of the velocity on the dispersion coefficient. In this example, $D_{R+} = 0.1$, $N_{Pe,I} = 200$, $R_I = R_m = t_+ = t_{+m} = t_p = 0.5$, $e_I = 0.1$, and $t_q = 0.41$.

The column was mounted in an ABI Model 230A HPEC system to use the unit's UV spectrophotometer which was located 15 cm from the bottom of the column. A Rainin back-pressure regulator was installed downstream of the detector to prevent outgassing in the detector and to control the pressure in the dialysis tubing. The fittings between the bottom of the bed and the detector flow cell (which had a volume of 7 μL) were Rainin flangeless fittings, and the tubing was 0.01 in. i.d. Teflon HPLC line.

The use of the dialysis tubing caused a few difficulties. Dehydrated dialysis tubing has permanent longitudinal creases that will create corner effects in the packed portion of the column unless the tubing is fully expanded. This is accomplished by increasing the pressure in the bed to about 5 psi. At this point, the tubing is slightly stretched. If the pressure gets too high, the bag will stretch too much and start to bulge slightly in places. This makes it difficult to pack under pressure so the two-step method discussed above was developed.

Also, the electric field lines curve due to the varying area of the chamber (see Figure 2), so that there is a small but significant radial component to the electric field that pushes the protein away from the center of the chamber. If the bed is not aligned properly, this radial force will act unevenly and the protein will be pressed against one side of the bed and will tend to smear along the membrane.

Experiments. The first experiment was the focusing of hemoglobin from dilute solution to a band of more concentrated protein to demonstrate that FGF is an equilibrium-gradient technique. The second experiment demonstrates the purification potential of FGF by separating two different oxidation states of myoglobin. The iron atom in the heme group of blood proteins can be found in the ferrous (2+) or ferric (3+) oxidation states. Ferromyoglobin (2+) can bind oxygen and will become *oxygenated* at even low oxygen partial pressure. However, prolonged exposure to oxygen will *oxidize* the molecule to ferrimyoglobin (3+) which can no longer bind oxygen. With the loss of an associated oxygen molecule, myoglobin turns from red to brown in color (Gurd, 1967; Stryer, 1988). Purification of the oxidized myoglobin (3+) (isolated myoglobin is generally in this form) often results in the formation of two bands as has been reported for

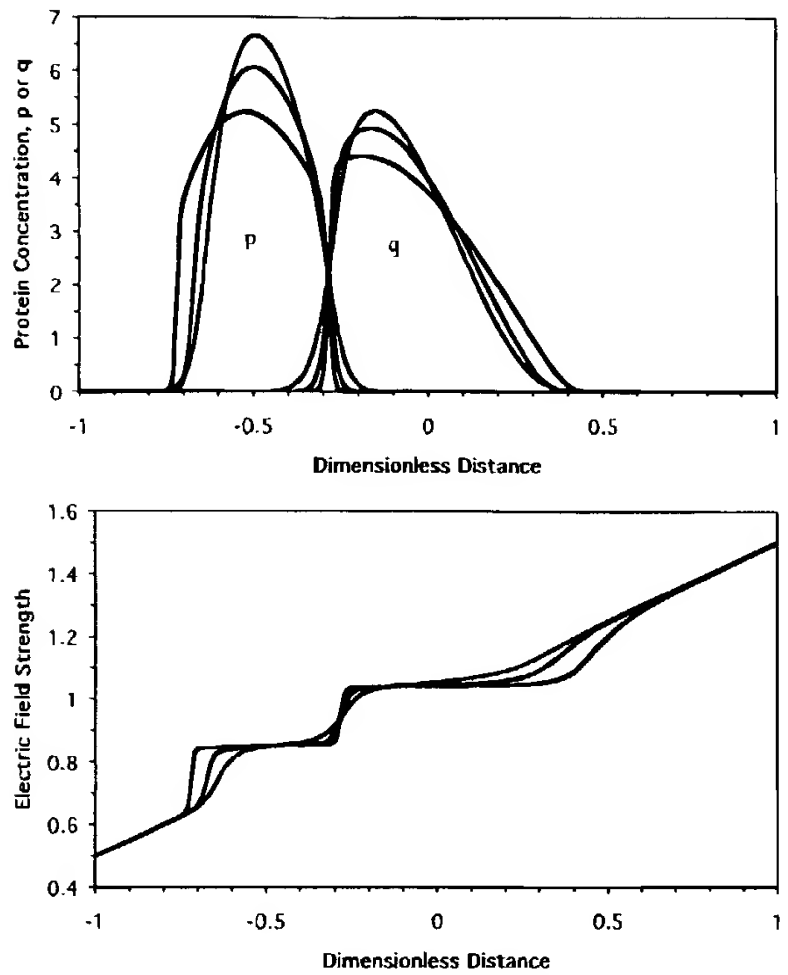

Figure 6. "Stacking out" of protein at high Peclet numbers ($N_{Pe,I}$ from 200 to 400 and 800). As the Peclet number is increased (while holding γ_p constant), the contiguous edges of the normalized protein bands become sharper and the bands tend to exclude each other because of electrostatic repulsion. Note that the forward edge of the front band also sharpens while the tail of the downstream band becomes more skewed. In this example, the two proteins have a 20% difference in mobility. $t_p = 0.1$, $t_q = 0.08$, $\gamma_p = 0.85$, and $\gamma_q = 1.06$. $D_{R+} = 0.1$, $e_I = 0.1$, and $R_l = R_m = t_+ = t_{+m} = 0.5$.

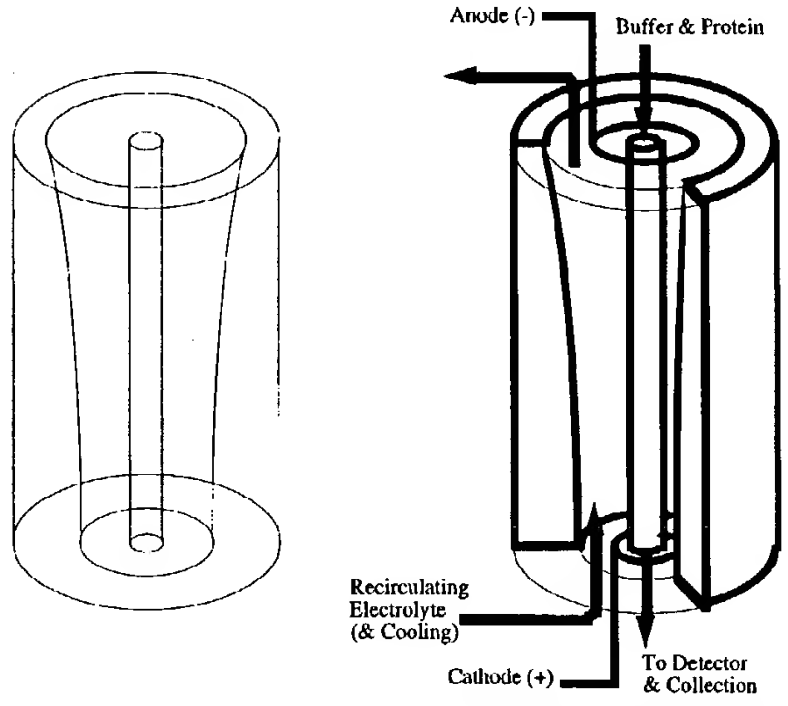

Figure 7. Simplified diagram of the experimental apparatus. In both figures, the inner surface of the outer shell is a shaped (fluted) Plexiglas cylinder and the narrow center tube is the dialysis tubing. The figure on the right shows the placement of electrodes and identifies the flows.

capillary zone electrophoresis (Rush et al., 1991) and isoelectric focusing (Rothgeb and Gurd, 1978). It has been proposed that the mechanism of the formation of the second band is the reduction of the oxidized myoglobin back to its native state. The formation of a second band also occurs during FGF, and its red color and faster

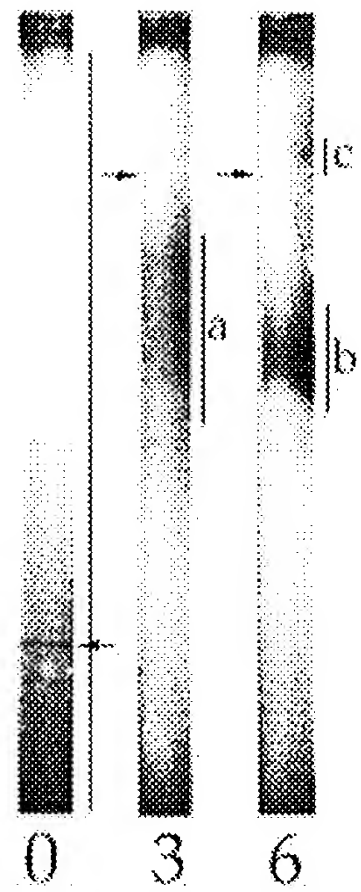

Figure 8. Focusing of hemoglobin. The gray cylinder in each picture is the packed bed. In the first picture ($t = 0$), the bed is completely filled with 0.1 wt % hemoglobin solution; the apparent gradation in shading from top to bottom is an artifact of the lighting used to take the slide. The next pictures show the progression to a focused band at 3 and 6 h. After 3 h, a pair of unresolved bands is visible just above the center of the apparatus (bracket a). In the last picture, the major band is focused just above the center mark (bracket b). There is also a secondary band near the top, focused on the left side of the bed (bracket c). The arrows mark an artifact of the scan; an adhesive joint in the Plexiglas is visible in the center of each scan.

mobility suggest that the brown ferrimyoglobin (3+ iron) is reducing to red oxyferromyoglobin (2+).

Both experiments were performed in a 10 mM Tris–26.6 mM glycine working buffer at pH 8.7 (room temperature) and a 5 mM Tris–13.3 mM glycine recirculating buffer. According to eq 9, an electric field gradient could also be created by using a conductivity gradient. It was hoped that the mismatch between the buffers would set up a conductivity gradient in the bed which, when superimposed on the "area-shaped" field, would act to tighten the protein bands. With the mismatch in place, there were fewer problems with the proteins focusing on the sides of the bed, but the bands were still somewhat asymmetrical.

Focusing of Hemoglobin. Focusing of hemoglobin (Sigma) was accomplished at a flow rate of 2.53×10^{-4} mL/s and a potential difference of 1000 V. The initial current was 12 mA, but this increased slowly over the course of the experiment, indicating that the conductivity of the recirculating buffer was increasing, probably due to diffusion from the more concentrated working buffer in the bed. The final current was 22 mA, 7 h after the electric field was turned on.

The experiment began by loading approximately 1 mL of a 0.1 wt % solution (approximately 1 mg) of hemoglobin onto the column. After the leading edge of the sample reached the bottom of the column, the field was turned on. Figure 8 is a series of pictures taken at different times showing the progressive focusing of hemoglobin from the 0.1 wt % solution. In the final picture, there is a second band above the major band whose identity is unknown.

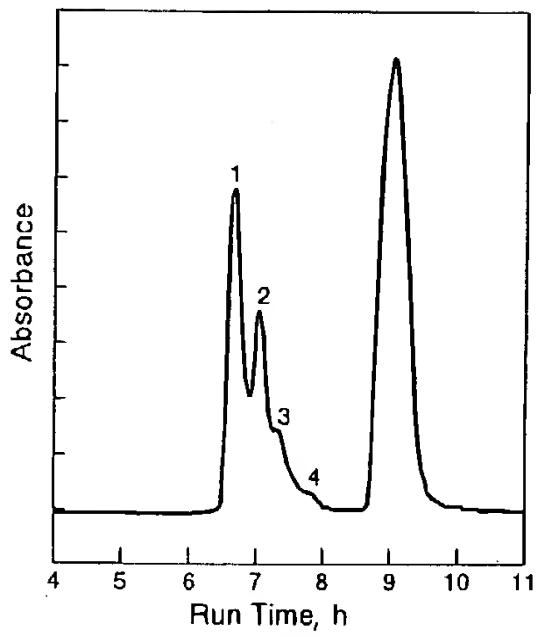

Figure 9. Absorbance trace at A280 from hemoglobin focusing experiment. Peak 1 is the focused hemoglobin band shown in bracket b of Figure 8. Peak 2 is the secondary band (Figure 8, bracket c), and the two remaining peaks are high-mobility species, possibly degradation products in the original sample, which focused very close to the top of the chamber. The trailing peak is a second pulse of hemoglobin, injected at 0.1 wt % concentration but not focused, and is shown for comparison. By comparing Figures 8 and 9, it is clear that a great deal of the resolution gained during focusing is lost during elution, probably due to extracolumn effects at the base of the focusing device.

After the protein focused, the field was turned off and the protein was eluted off the column to the spectrophotometer. A second pulse of approximately 1 mL of 0.1% hemoglobin was then run through the column without focusing for comparison. Figure 9 shows the absorbance trace at 300 nm of the run. Assuming a linear correspondence between concentration and absorbance, at least a 2-fold increase in protein concentration can be estimated from the relative heights of the two peaks.

An additional hemoglobin focusing experiment was performed to check the distribution inside the bed. Instead of eluting to the detector after the hemoglobin focused, the apparatus was disassembled and the bed frozen. Cutting the bed longitudinally revealed that, although the hemoglobin was distributed in a band all the way around the bed, it did not penetrate into the interior of the bed deeper than about 2 mm from the surface of the membrane. Apparently, due to the radial component of the electric field mentioned earlier, proteins are drawn toward the surface of the dialysis tube by the field and tend to remain there.

Separation of Myoglobins. Separation of myoglobins with different oxidation states was accomplished at the same buffer conditions as the hemoglobin experiment and, once again, at a voltage of 1000 V. As before, the current increased from 12 to 20 mA during the 7 h the field was applied.

The experiment began by loading about 0.3 mL of a 0.5 wt % horse-heart myoglobin (Sigma) solution into the top half on the chamber (1.5 mg). At this point all of the protein was in the brown, oxidized form. The field was turned on, and the protein focused at the top of the column with a flow rate of 0.37×10^{-4} mL/min. Reduction of the 3+ iron occurred faster when the myoglobin was focused at the top of the chamber. After about 1 h, a second band of reddish myoglobin began to form above the other band. When this second band was well established (about 2 h), the flow rate was increased to 1.83×10^{-4} mL/s and the bands were refocused near the bottom of the chamber. The bands were held there for about 2 h more until they were of about equal concentration.

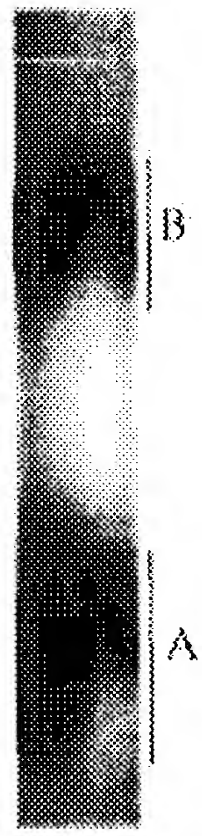

Figure 10. Separation of oxidized and reduced myoglobins. This picture is a closeup of the final steady-state distribution of myoglobin in a second focusing experiment. Band A is the oxidized form of myoglobin (Fe^{3+}). Band B above that is the reduced form (Fe^{2+}) and is distinctly redder in color in the original photographs. This experiment illustrates that proteins with a single charge difference can be separated using this apparatus.

A picture of the focused myoglobin bands is shown in Figure 10. The bands were clearly separated by about 2.5 cm although there is a murky area between the bands, probably consisting of reduced myoglobin moving from one band to the other. There were also two other bands above these major bands of which are not visible in this closeup. These may have been isoforms of myoglobin, contaminants, or degradation products. After steady-state was reached, the electric field was turned off and the bands were then eluted from the column and passed through a UV detector. A second pulse of the original myoglobin sample was run through the column for comparison. The absorbance trace at 300 nm is shown in Figure 11.

The peaks on the absorbance traces (Figures 9 and 11) were not as sharp as would be expected from the photographs. However, very sharp peaks could be obtained on the first run of a newly packed column. This indicates that the extra dispersion which occurs with repeated operation of the column has something to do with changes in the packing as it is used. It may be that the electric field is physically changing the beads, in which case a different packing must be found. Or, it may be that the beads are redistributing themselves due to the electric field or as the membrane tubing slowly expands under the pressure exerted by the flow.

As is apparent in Figure 10, the solute bands are distorted into a z-shaped pattern around the perimeter of the dialysis tube. We believe that this is an artifact introduced by nonuniformities in the tube itself, i.e., standard laboratory dialysis tubing is creased during packaging and is slightly bowed, even when stretched and filled with packing. Protein tends to collect in these nonuniformities, and because they also disturb the flow,

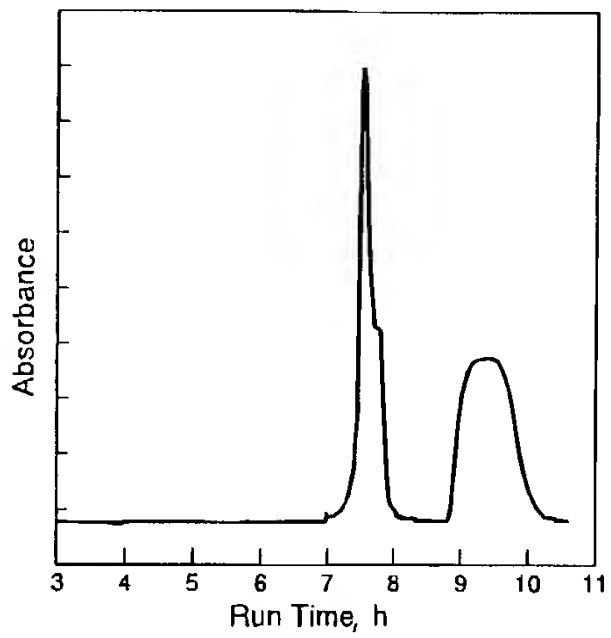

Figure 11. Absorbance trace at A280 of separated myoglobins. The leading peak corresponds to the oxidized ferrimyoglobin (Fe^{3+}), and the shoulder on this peak is the reduced ferromyoglobin (Fe^{2+}). The trailing peak is the unfocused sample at 0.5 wt % concentration and is shown for comparison. As in Figure 9, it is believed that extracolumn effects are responsible for the loss of resolution between the focused and the eluted bands.

they slightly shift the position of the focal point. These problems could be substantially reduced by using specialty dialysis tubing or by developing a frame for the membrane which would force it into the shape of a perfect right cylinder.

Comparison To Model Predictions. These experiments demonstrate that FGF is an equilibrium gradient technique and can be used to focus and separate proteins. It now remains to see how well the complex model can predict the location and shape of the protein peaks. Although all parameters were determined from literature or experimental measurements, i.e., there was no empirical fitting, their values are approximate so our evaluation of the model is only qualitative. Also, it is apparent that the assumption of constant radial protein concentrations does not agree with the experimentally determined distribution in the bed.

The physical dimensions of the apparatus are given in Table 1. The open area of the packed bed was estimated by assuming a void fraction of one third. The buffer parameters are summarized in Table 2. The diffusion coefficient of the cation was calculated from its mobility coefficient using the Nernst–Einstein equation eq 64. The concentration of the buffer in region 2 was 5 mM Tris–13.3 mM glycine. The fraction of each component ionized at pH 8.7 was calculated from published pK_a's. The concentration of the ions was then averaged, yielding an ionic strength of 1.23 mM. Because the working buffer entered the chamber at twice the concentration of the recirculating buffer, the cation concentration on the packed-column entrance boundary condition was multiplied by 2.

The values of the remaining parameters used in modeling the experiments are given in Tables 3 and 4. The ionic mobility of hemoglobin and the oxidized ferrimyoglobin were estimated in the lab by electrophoresis in an agarose gel at the same buffer conditions as the experiments. The charges on these proteins were estimated from titration curves (Mosher et al., 1992; Breslow and Gurd, 1962). The charge and ionic mobility of the ferromyoglobin were estimated from the ferrimyoglobin parameters assuming that it had exactly one more positive charge.

Table 1. Physical Dimensions of Equipment

characteristic length (cm)	L	8.26
area of phase 1 (cm^2)[a]		0.317
void area of phase 1 (cm^2)[b]	A_1	0.106
area at $x = -L$ (cm^2)	A_L	11.2
area at $x = L$ (cm^2)	A_R	2.64
interfacial width (cm)	W	1.99
membrane thickness (cm)[c]	δ	0.005

[a] Based on prepressurized diameter. [b] Based on an estimated void fraction of $^1/_3$. [c] Estimated.

Table 2. Buffer Parameters

cation charge	z_+	1
anion charge	z_-	−1
cation mobility coefficient (cm^2/(V s))[a]	ω_+	2.41×10^{-4}
anion mobility coefficient (cm^2/(V s))[a]	ω_-	4.10×10^{-4}
cation diffusion coefficient (cm^2/s)[b]	D_{+m}	6.19×10^{-6}
ionic concentrations in region 2 (mol/cm^3)[c]	$c_{+2} = c_{-2}$	1.23×10^{-6}

[a] From Table 5-1 of Mosher et al. (1992). [b] Calculated from the mobility coefficient using the Nernst–Einstein equation (eq 65). [c] Average of cation and anion concentrations calculated from the pK_a's (Koegler, 1994).

Table 3. Parameters for Hemoglobin Focusing

charge[a]	z_p	−20
ionic mobility (cm^2/(V s))[b]	μ_p	6.20×10^{-5}
bulk flow rate (cm^3/s)		2.53×10^{-4}
solute velocity (cm/s)[c]	u_1	2.40×10^{-3}
column dispersion (cm^2/s)[d]	D_l	2.25×10^{-5}
total current (A)	I_T	0.012

[a] From Table 7-4 of Mosher et al. (1992). [b] Measured in an agarose gel at pH 8.7. [c] Bulk flow divided by the void area of phase 1. [d] Estimated as μ_1 times the particle diameter times 2.

Table 4. Parameters for Myoglobin Separation

charge on ferrimyoglobin (3+)[a]	z_p	−2.72
charge on ferromyoglobin (2+)[b]	z_q	−1.71
ionic mobility of ferrimyoglobin (cm^2/(V s))[c]	μ_p	3.70×10^{-5}
ionic mobility of ferromyoglobin (cm^2/(V s))[b]	μ_q	5.06×10^{-5}
bulk flow rate (cm^3/s)		1.83×10^{-4}
solute velocity (cm/s)[d]	u_1	1.73×10^{-3}
column dispersion for all solutes (cm^2/s)[e]	D_l	1.60×10^{-5}
total current (A)	I_T	0.012

[a] From Figure 3 from Breslow and Gurd (1962). [b] Estimated from ferrimyoglobin. [c] Measured in agarose gel at pH 8.7. [d] Bulk flow divided by the void area of phase 1. [e] Estimated as μ_1 times the particle diameter times 2.

Packing interstitial velocities were estimated by dividing the experimental space velocity by the void area of the bed. Column dispersion in chromatography can usually be estimated as somewhere between 1 and 2 times the velocity times the particle diameter of the packing. Because of the extra dispersion seen in the absorbance traces, the larger dispersion was chosen for modeling. The initial value of the total current was chosen for the simulation because the initial buffer concentrations were used.

The results of the modeling are depicted graphically in Figures 12 and 13. When comparing these graphs to the experimental results, the left boundary corresponds to the top of the column and the right boundary to the bottom. The model predicts that the cation and anion concentrations in the working buffer drop almost immediately to the recirculating buffer concentration and that the conductivity mismatch has no effect on the electric field. The model does predict that all the proteins will focus in the chamber near the locations seen in the experiments. The hemoglobin peak is a little downstream of where it is seen in the experiments, but the

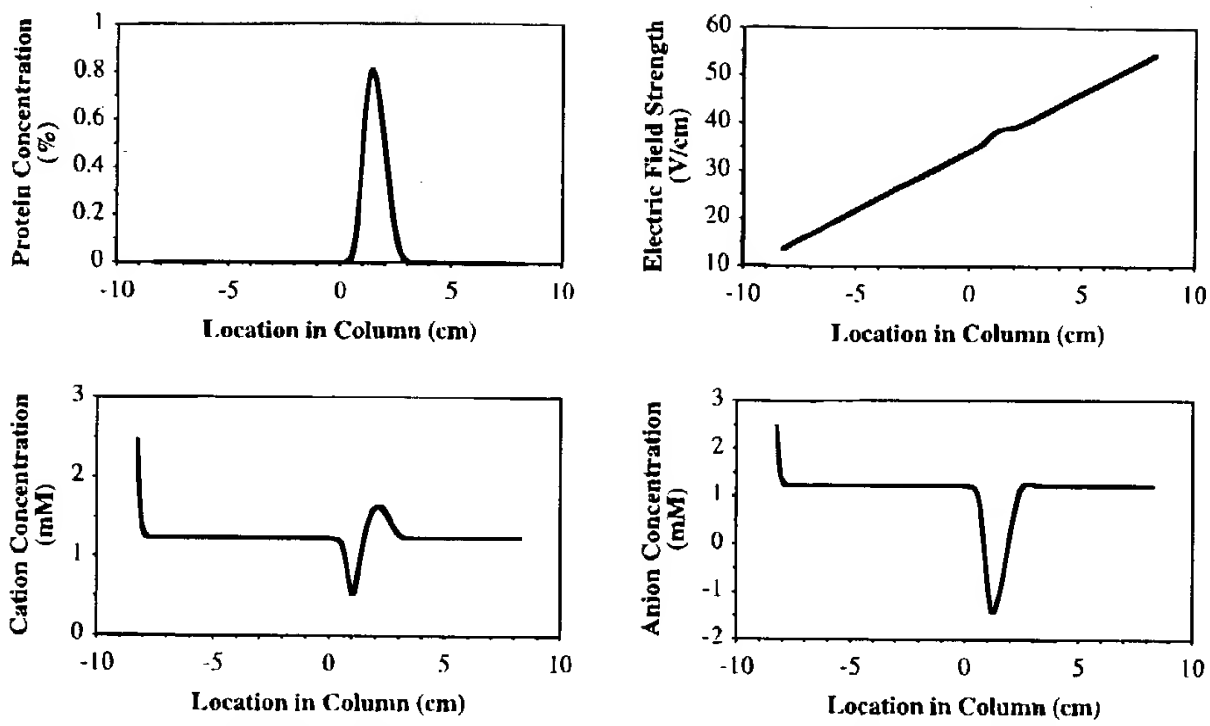

Figure 12. Simulation of hemoglobin focusing experiment using the nonlinear model. Note that the model predicts that the band will focus just below the midpoint of the apparatus, while in the experiment, it focuses just above the center. This discrepancy is most likely due to a low estimate of the free solution electrophoretic mobility of hemoglobin, e.g., the hemoglobin may have been slowed by the agarose gel used in our mobility experiments. In addition, the anion concentration drops below zero, indicating that the experiment is taking place in a regime where the model cannot accurately predict anion behavior. This is probably due to the fact that the buffer is not allowed to shift pH. Simulation parameters are given in Tables 1, 2, and 4.

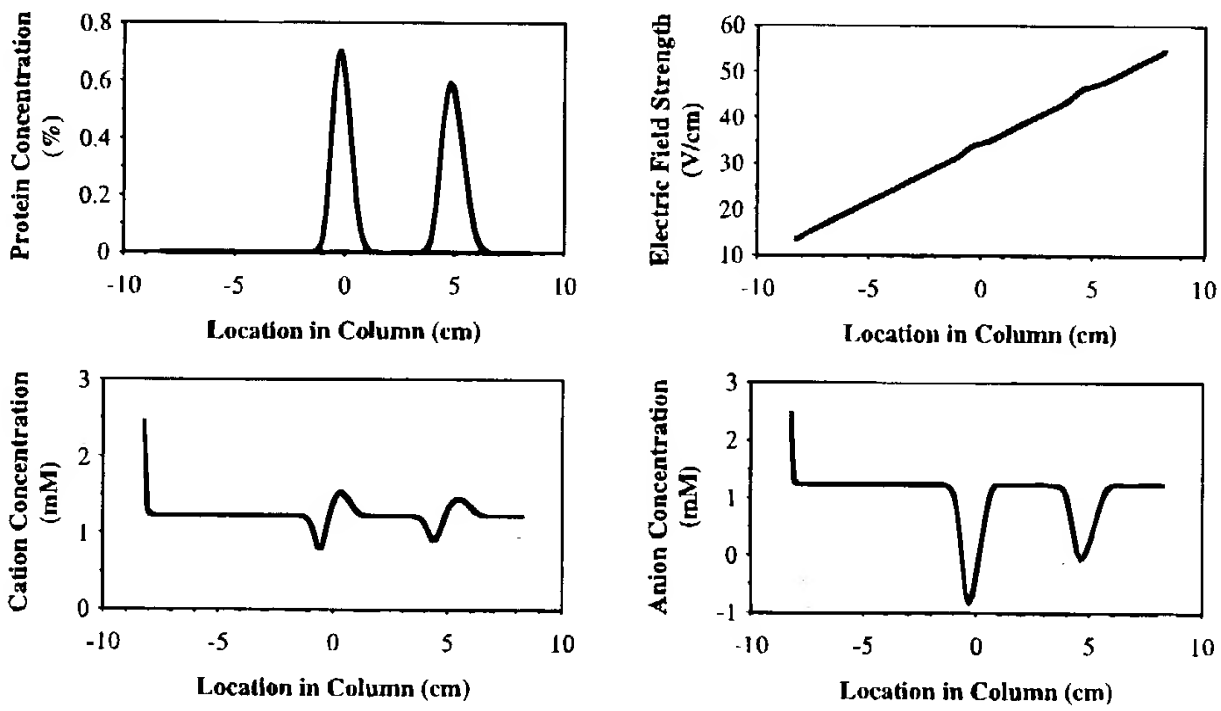

Figure 13. Simulation of myoglobin separation experiment using the nonlinear model. In this case, experiment and theory are in close agreement with respect to the location of the focused peaks. Parameters are given in Tables 1, 3, and 4.

myoglobin peaks are very close to the experimental locations.

Discrepancies in peak location between experimental results and the simulations are most probably due to the approximate nature of the parameters. The concentrations predicted by the models in both cases are about a factor of 2 greater than seen in the experiments, implying a source of dispersion not accounted for in the theory.

The model does not adequately predict the shape of the focused bands. In the experiments, the downstream edges of the protein bands were much sharper than the upstream edges. The nonlinear model predicts that this should occur when the ionic velocities of the proteins are higher than the anion, but at this pH, the partially ionized glycine is probably still much faster than the larger proteins. The shape of the bands seen in the experiments may have something to do with radial component of the electric field since the protein is not spread uniformly across the radius of the bed but is, in fact, really focusing very near the membrane.

Under the conditions used in the experiments, our model predicts that the anion concentration becomes negative where the protein is focusing. This indicates that the model as it is formulated cannot make accurate predictions at high protein concentrations where the pH and the conductivity may change abruptly. This shortcoming of the model may be due to neglect of the properties of the weak electrolytes, i.e., more of the Tris may dissociate at this point to compensate for the predicted excess of negative charges. Adding all charged states of the buffer components to the model and allowing them to interconvert might alleviate this fault. This would allow the model to predict possible pH shifts in the neighborhood of the protein bands but would also make it far more difficult to solve numerically.

Conclusions

Equilibrium gradient methods hold great promise in bioprocessing because they can combine the steps of isolation and concentration. They can also be adapted to a separation as needed by choosing appropriate counteracting forces based on the differences in the specific proteins involved. Field gradient focusing is a new addition to this class of separation techniques with the unique property of using a gradient in the electric field, instead of a gradient in the flow or pH, to focus proteins.

Our experiments verify that FGF is an equilibrium gradient method. In a first set of experiments, hemoglobin was focused from dilute solution to a concentrated band, and in a second set, different oxidation states of myoglobin were separated. These experiments demonstrate that FGF has the power to separate proteins that differ by only one charge on at least a milligram scale and can do so using simple buffers rather than ampholytes.

The mathematical model presented here *qualitatively* predicts the location and concentration of the focused protein peaks at steady-state. Unfortunately, it also predicts that anion concentrations go negative in the focusing region at high currents, indicating that the model is too simplistic to make accurate quantitative predictions. This is probably because the model treats the ionized fraction of the buffer salts as strong electrolytes and therefore does not allow for variations in the charged states of the buffer ions or the pH. This modification requires the inclusion of quite a few additional equations to the model to account for the alternative charged and uncharged states and this will make numerical solution more difficult.

The small perpendicular component of the electric field which caused hemoglobin to focus into a donut-shaped ring adjacent to the membrane surface rather than as a uniformly distributed plug appears to be an integral part of the technique that will be difficult to engineer out of this apparatus. This implies that this device will scale with the perimeter of the packed bed rather than the cross-sectional area. For this and the other reason cited above, we expect that FGF in packed beds will not scale to capacities greater than about 100 mg. However, it is possible that this class of techniques could be applied at virtually all scales by engineering them into device geometries which can deal effectively with heat dissipation and which do not suffer from transverse field effects, e.g., the recycle electrophoresis devices (Bier, 1986; Ivory, 1990) or membrane-based electrophoretic devices (Righetti et al., 1990; Shea et al., 1994; Margolis et al., 1995).

Temperature excursions, which are not included in our model, might have an important secondary effect on performance via two mechanisms: variations in the pH and in the viscosity of the buffer changing the local value of the protein's electrophoretic mobility. Under the conditions used in these experiments, the maximum power dissipation at the constricted (lower) end of the apparatus was about 2 W/cm^3, giving a radial temperature variation of roughly 10 °C at that point. At the center of the column near the point where the bands were focused in these experiments, this variation is about 2 °C from the center to the wall of the dialysis tube. A 10 °C increase in temperature will cause a 30% decrease in the viscosity (which is inversely proportional to the electrophoretic mobility) and a 0.1 unit decrease in the pH which will decrease the mobility of hemoglobin by about 3%.

The net result of this "worst-case" scenario is that the temperature excursions associated with field-gradient focusing could lead to marked dispersion of the solute bands, primarily because of variations in buffer viscosity with temperature. This is very different from IEF in which spatial variations in the pH with temperature are the dominant form of dispersion after diffusion. In the experiments described above, dispersion associated with spatial temperature variations is further mitigated by the fact that the protein is distributed in an annulus near the membrane surface and sees only a small fraction of the maximum temperature excursion.

Future Directions

Given the complexity of the equipment and protocols used in this work and considering the nagging problem of radial current distribution, future research in this area will move toward designing a more flexible and "user-friendly" apparatus. Although it was not discussed in this paper, FGF has an advantage over the other techniques in its class is that, unlike the steady-state pH gradients used in IEF or the fixed K_{av} (MWCO) gradients integral to CACE, it is possible to manipulate the electric field gradient from outside the column by using a plurality of independent electrodes instead of the shaped chamber described in this paper. This allows the possibility that the field could be dynamically "shaped" during a run to improve performance. For instance, one can imagine a scenario where the field gradient is steep during the sampling period of a run to speed loading, then shallow or multiplateaued during the fractionation phase, and finally, the field gradient could be made steep to concentrate products prior to removal or even locally reversed to speed individual peaks out of the chamber.

In addition, it is our belief that other, as yet undiscovered, members of this class of techniques remain to be found, developed, and exploited.

Acknowledgment

This material is based on W.K.'s MS work at WSU which was supported under a National Science Foundation Graduate Research Fellowship. We wish to thank Bill Gobie for allowing W.K. to use his subroutine, ODECOL, to solve her mathematical model.

a	dimensionless concentration of anion
A	total cross-sectional area (cm^2)
$A_k(x)$	local cross-sectional area of the kth region (cm^2)
A_B	total cross-sectional area of chamber at the bottom ($x = L$) (cm^2)
A_R	equation describing the ratio of the area of region 2 to the area of region 1
A_T	total cross-sectional area of chamber at the top ($x = -L$) (cm^2)
c	dimensionless concentration of cation
$c_i(x)$	concentration of ion, i (mol/cm^3)
$c_{ik}(x)$	concentration of ion, i, in the kth region (mol/cm^3)
$c_{p,av}$	average concentration of protein, p (mol/cm^3)
D_i	dispersion coefficient of ion, i (cm^2/s) (subscript m denotes value in membrane)
D_{R+}	dimensionless parameter, ratio of diffusion coefficient of cation in the membrane to the dispersion coefficient in the column
e_R	dimensionless parameter, ratio of average charge contribution of protein to charge contribution of buffer ions
$E(x)$	local electric field strength (V/cm)
E_0	average electric field strength (V/cm)

E_1	slope of electric field gradient (V/cm^2)
F	Faraday's constant = 96 494 C/mol
$i_k(x)$	charge density or charge flux in the kth region (A/cm^2 or C/(cm^2 s))
I	total current (A)
$J_{ik}(x)$	molar flux of ion, i, in the kth region (mol/(cm^2 s))
K	dimensionless parameter, collection of physical dimensions of apparatus
L	characteristic length equal to one-half the length of the chamber (cm)
$M_i(x)$	total moles of species i up to point x (mol)
M_{pT}	total moles of protein, p, present in chamber (mol)
N_k	number of components in the kth region
$N_{Pe,i}$	Peclet number for component i
$p(z)$	dimensionless concentration of protein, p
R_1	dimensionless parameter, ratio of area of region one to total area
t_i	dimensionless parameters, ratio of mobility of ion, i, to total mobility of buffer
$u_k(x)$	convective velocity of medium in the kth region (cm/s)
v_i	electrophoretic velocity of a migrating ion, i (cm/s)
W	width of the interface between regions 1 and 2 or the membrane perimeter (cm)
x	axial coordinate
z_i	charge of ion, i

Greek Symbols

δ	membrane thickness (cm)
γ_p	dimensionless parameter, the ratio of convective velocity to the average electrophoretic velocity of protein, p, in the column
μ_i	ionic mobility of ion, i (cm^2/(V s)) (subscript m denotes value in membrane)
σ	conductivity (C/(V cm s))
σ^2	variance (cm^2)
ω_i	mobility of ion, i (cm^2/(V s))
χ_i	focal point, cm

Acronyms

CACE	counteracting chromatographic electrophoresis
FGF	field gradient focusing
IEF	isoelectric focusing
K_{AV}	size exclusion chromatography distribution coefficient
MWCO	molecular weight cutoff

Literature Cited

Ascher, U.; Christiansen, J.; Russell, R. D. ALGORITHM 569, COLSYS: Collocation Software for Boundary-Value ODEs [D2]. *ACM Trans. Math. Software* **1981**, *7*, 223–229.

Bier, M. Scale-Up of Isoelectric Focusing. *ACS Symposium Series: Separation, Recovery, and Purification in Biotechnology*; Asenjo, J. A., Hong, J., Eds.; American Chemical Society: Washington, DC, 1986; Chapter 13.

Boncinelli, E.; Simeone, A.; et al. An Agarose Gel Resolving a Wide Range of DNA Fragment Lengths. *Anal. Biochem.* **1983**, *134*, 40–43.

Breslow, E.; Gurd, F. R. N. Reactivity of Sperm Whale Met-myoglobin towards Hydrogen Ions and *p*-Nitrophenyl Acetate. *J. Biol. Chem.* **1962**, *237*, 371.

Everaerts, F. M.; Verheggen, T. P. E. M. Capillary Isotachophoresis. In *New Directions in Electrophoretic Methods*; Jorgenson, J. W., Phillips, M. American Chemical Society: Washington, DC, 1987; Vol. 335, pp 199–221.

Everaerts, F. M.; Mikkers, F. E. P.; et al. Isotachophoresis: Theory, Instrumentation and Applications. *J. Chromatogr. Library*; Elsevier Publishing Co.: Amsterdam, 1976; Vol. 6.

Giddings, C. J. Two-Dimensional Separations. *Anal. Chem.* **1984**, *56* (12), 1258.

Giddings, J. C.; Dahlgren, K. Resolution and Peak Capacity in Equilibrium–Gradient Methods of Separation. *Sep. Sci. Technol.* **1971**, *6*, 345.

Gobie, W. A.; Ivory, C. F. Continuous Counter-Acting Chromatographic Electrophoresis. *Biotechnol. Prog.* **1990**, *6* (1), 21.

Gurd, F. R. N. Myoglobins. In *The Encyclopedia of Biochemistry*; Williams, R. J., Lansford, E. M., Jr., Eds.; Reinhold Publishing Corp.: New York, 1967.

Hjertén, S.; Mohammad, J.; et al. High-Performance Chromatofocusing of Proteins on Compressed Continuous Beds with Improved Properties. *Biotechnol. Appl. Biochem.* **1992**, *15*, 247–256.

Ivory, C. F. The Prospects for Large-Scale Electrophoresis. *Special Issue on Bioseparations*; Ivory, C. F., Ed.; Marcel Dekker, Inc.: New York, 1988; Vol. 23, p 875.

Ivory, C. F. The Development of Recycle Zone Electrophoresis. *Electrophoresis* **1990**, *11*, 919–926.

Jorgenson, J. W., Phillips, M., Eds. *New Directions in Electrophoretic Methods*; ACS Symposium Series; American Chemical Society: Washington, DC,, 1987.

Jungbauer, A.; Tauer, C.; et al. Isolation of Isoproteins from Monoclonal Antibodies and Recombinant Proteins by Chromatofocusing. *J. Chromatogr.* **1990**, *512*, 157–163.

Koegler, W. S. Zone Electric Field Gradient Focusing: A Novel Techniques for Protein Separation. M.S. Thesis, Washington State University, 1994.

Kuhr, W. G.; Monnig, C. A. Capillary Electrophoresis. *Anal. Chem.* **1992**, *64* (12), 389R–407R.

Lochmüller, C. H.; Ronsick, C. S. Isoelectric Focusing with Thermally Formed, Stepped-Ramp pH Gradients: Separation of Human Hemoglobin Variants A and S. *Anal. Chim. Acta* **1991**, *249*, 297–302.

Margolis, J.; Corthals, G.; et al. Preparative Reflux Electrophoresis. *Electrophoresis* **1995**, *16*, 98–100.

Mattock, P.; Aitchison, G. F.; et al. (1980). Velocity Gradient Stabilized, Continuous, Free Flow Electrophoresis. A Review. *Sep. Purif. Methods* **1980**, *9* (1), 1.

McCoy, B. J. Counteracting Chromatographic Electrophoresis and Related Imposed-Gradient Separation Processes. *AIChE J.* **1986**, *32*, 1570.

Mosher, R. A., Saville, D. A.; Thormann, W. *The Dynamics of Electrophoresis*; VCH Publishers, Inc.: New York, 1992.

Nath, S.; Schütte, H.; et al. Application of Continuous Zone Electrophoresis to Preparative Separation of Proteins. *Biotechnol. Bioeng.* **1993**, *42*, 829–835.

O'Farrell, P. H. Separation Techniques Based on the Opposition of Two Counteracting Forces to Produce a Dynamic Equilibrium. *Science* **1985**, *227*, 1586.

Pawliszyn, J.; Wu, J. Ampholyte-Free Isoelectric Focusing of Proteins in Cone Shaped Capillaries. *J. Microcolumn Sep.* **1993**, *5* (5), 397–401.

Pohl, H. A. *Dielectrophoresis: The Behavior of Neutral Matter in Nonuniform Electric Fields*; Cambridge University Press: Cambridge, 1978.

Righetti, P. G. *Isoelectric Focusing: Theory, Methodology and Applications*; Elsevier Biomedical Press: Amsterdam, 1983.

Righetti, P. G.; Wenisch, E.; et al. Preparative Purification of Human Monoclonal Antibody Isoforms in a Multi-Compartment Electrolyser with Immobiline Membranes. *J. Chromatogr.* **1990**, *500*, 681–696.

Righetti, P. G.; Faupel, M.; et al. Preparative Electrophoresis With and Without Immobilized pH Gradients. *Advances in Electrophoresis*; Chrambach, A., Dunn, M. J., Radola, B. J., Eds.; VCH: New York, 1991; Vol. 5, pp 159–200.

Rolchigo, P. M.; Graves, D. J. Analytical and Preparative Electrophoresis in a Nonuniform Electric Field. *AIChE J.* **1988**, *34* (3), 483–492.

Roman, M. C.; Brown, P. R. Free-Flow Electrophoresis as a Preparative Separation Technique. *Anal. Chem.* **1994**, *66*, 86A–94A.

Rothgeb, T. M.; Gurd, F. R. N. Physical Methods for the Study of Myoglobin. In *Methods in Enzymology*; Fleischer, S., Packer, L., Eds.; Academic Press: New York, 1978.

Rush, R. S.; Cohen, A. S.; Karger, B. L. Influence of Column Temperature on the Electrophoretic Behavior of Myoglobin and a-Lactalbumin in High Performance Capillary Electrophoresis. *Anal. Chem.* **1991**, *63*, 1346.

Schwartz, D. C.; Cantor, C. R. Separation of Yeast Isolation Chromosome-sized DNAs by Pulsed Field Gradient Gel Electrophoresis. *Cell* **1984**, *37*, 67.

Scragg, A. H. In *Biotechnology for Engineers*; Scragg, A. H., Ed.; John Wiley & Sons: New York, 1988.

Shea, L. D.; Feke, D. L.; et al. Counteracting Flow Electrophoresis: A Technique for Separating Biochemicals or Charged Macromolecules. *Biotechnol. Prog.* **1994**, *10*, 246–252.

Sikdar, S. K., Bier, M., Todd, P., Eds. *Frontiers in Bioprocessing*; CRC Press, Inc.: Boca Raton, FL, 1990; pp 2–13.

Sluyterman, L. A.Æ.; Kooistra, C. Change of Counterion Concentration and of Resolving Power in a Chromatofocusing Run. *J. Chromatogr.* **1990**, *519*, 217–220.

Southern, E. M. A Preparative Gel System for Large Scale Separations. *Anal. Biochem.* **1979**, *100*, 304.

Stryer, L. *Biochemistry*, 3rd ed.; W. H. Freeman & Co.: New York, 1988.

van Holde, E. K. *Physical Biochemistry*; Prentice-Hall, Inc.: Englewood Cliffs, NJ, 1971.

Accepted August 1, 1996.[⊗]

BP960062M

[⊗] Abstract published in *Advance ACS Abstracts*, September 1, 1996.